Pergamon

PII: S0146-6380(96)00066-6

Org. Geochem. Vol. 24, No. 8/9, pp. 913–920, 1996

0146-6380/96 $15.00 + 0.00

$\delta^{13}C$ compositions of saturate and aromatic fractions of lacustrine oils and bitumens: evidence for water column stratification

J.W. COLLISTER and D.A. WAVREK

Earth Sciences and Resources Institute, Geochemistry Unit, Department of Civil and Environmental Engineering, University of Utah, 421 Wakara Way, Suite 125, Salt Lake City, Utah 84108, U.S.A.

(Received 22 November 1995; returned to author for revision 26 April 1996; accepted 22 May 1996)

Abstract—Saturate fractions of oils and source rocks are generally depleted in ^{13}C relative to the aromatic fraction. The isotopic difference between these two fractions ($\Delta\delta_{aro\text{-}sat}$) is largest typically in lacustrine oils and bitumens, and smallest in marine samples. Depletions of ^{13}C in saturate fractions in samples from three lacustrine basins (China, Argentina and U.S.A.) correlate strongly with hopane abundance. Extremely ^{13}C depleted hopanes have been documented in ancient and modern lacustrine settings and are explained by input from methanotrophic bacteria. As these bacteria thrive at the chemocline of stratified lakes, extremely ^{13}C depleted hopanes in geologic samples is evidence for paleostratification. Comparatively low $\Delta\delta_{aro\text{-}sat}$ values in marine samples are related to abundant sulfate in marine environments, since sulfate reducers out-compete methanogens for metabolic intermediates and attenuate the methane cycle. The strong positive correlation of quantitative hopane abundance with the ^{13}C-depletion in saturate fractions of lacustrine samples provides circumstantial evidence for biogenic input from methanotrophic bacteria and for stratified water columns during source rock deposition. Further, this observation explains why the "Sofer-plot" effectively differentiates stratified lacustrine samples from open marine and non-stratified lacustrine samples. The wide distribution of our sample set suggests that this is a global phenomenon. Copyright © 1996 Elsevier Science Ltd

Key words—carbon isotopes, irm–GC–MS, methanotrophic bacteria, methane cycle, lacustrine geochemistry, stratification, Sofer-plot

INTRODUCTION

Carbon isotopic variations among fractions of crude oils have long been recognized. Commonly, a progressive enrichment in ^{13}C is observed with increasing polarity of compounds relative to the saturated hydrocarbons (Stahl, 1978; Chung *et al.*, 1981). Based on this observation, isotope-type-curves ($\delta^{13}C$ vs compound class) are used routinely to infer genetic relationships between oils and to compare oils to potential source rocks (Stahl, 1978; Chung *et al.*, 1981). Sofer (1984) noted that the $\Delta\delta_{aro\text{-}sat}$ value (‰) is, on average, lowest in marine oils and used this observation to differentiate "waxy" (terrigenous) oils from "non-waxy" (marine) oils. In that study, empirical observation showed a cross-plot of $\delta^{13}C_{saturates}$ vs $\delta^{13}C_{aromatics}$ can differentiate marine and non-marine oils with a best separation line having the formula $\delta^{13}C_{aro} = 1.14\delta^{13}C_{sat} + 5.46$ (Sofer, 1984).

SAMPLES

A suite of samples of lacustrine sourced crude oils and lacustrine potential source rocks (Table 1) were analyzed. These include samples from China, Argentina and the United States. Samples from the Green River Formation are from the Shell 22X-1 (U.S.G.S. C177) core and are described in detail elsewhere (Collister *et al.*, 1992). Samples from the Cuyo Basin (Argentina) include one potential source rock (Cacheuta Formation) and four crude oils. The remaining six crude oils are from a non-marine basin in the Peoples Republic of China.

METHODS

Total extractable organic material was obtained by Soxhlet extraction with dichloromethane for 24–72 h. Excess solvent was removed by rotary evaporation at 24–30°C. The oils were topped for 18–21 h at 60°C. The oils and bitumens were chromatograpically fractionated using a stationary phase of silica gel (100–200 mesh activated at 100°C overnight) and mobile phases of *n*-hexane (saturated hydrocarbon fraction), toluene (aromatic fraction), and methanol (NSO fraction). In the case of the Green River bitumens, previously isolated neutral fractions (Collister *et al.*, 1992) were fractionated chromatographically. Carbon isotopic compositions of the resulting saturate and aromatic fractions were determined by Coastal Laboratories (Austin, Texas).

Saturated hydrocarbon fractions were analyzed by flame ionization capillary gas chromatography and gas chromatography–mass spectrometry (GC–MS). Analytical conditions were: split injection (50:1) on a

60 m × 0.25 mm i.d. DB-1 fused silica capillary column (0.25 mm film thickness) held isothermal for 2 min then programmed from 35°C to 310°C at 2°/min followed by a 70.5 min isothermal hold time. Saturated hydrocarbon fractions were analyzed by electron impact GC–MS in the selected ion monitoring (SIM) mode using a Hewlett Packard 5870 MSD. To obtain spectra for individual compounds, a subset of samples was also analyzed in the full scan mode. Absolute concentrations of individual compounds were calculated relative to a surrogate standard (5b-cholane). Response factors for hopanoid compounds relative to the surrogate standard were determined by GC–MS analysis of a mixture of 17a(H),21b(H)-hopane, 17b(H),21a(H)-moretane and 5b-cholane standards in varying concentrations.

Carbon isotopic compositions of individual components in saturate fraction of the Green River bitumens were determined using irm–GC–MS (Matthews and Hayes, 1978; Merritt *et al.*, 1994). On-column injection was employed and the GC column was programmed from 60–230°C at 3°/min and from 230–320°C at 2.5° min with a final hold time of 45 min (He carrier gas). A Hewlett Packard Ultra-1 column (50 m × 0.32 mm i.d., 0.5 mm polymethylsilicone cross-linked bonded phase) was used for these analyses.

RESULTS AND DISCUSSION

Carbon isotopic compositions of saturate and aromatic fractions for the oils and bitumens are summarized in Table 2. These data, along with published data from other lacustrine basins, are plotted on the so-called "Sofer-plot" (Fig. 1). With the exception of one Chinese lacustrine oil, all the samples plot above the best-fit line (Sofer, 1984) that separates oils sourced from open marine vs non-marine sequences. Isotopic variations between

Table 1. List of crude oil samples and sedimentary rock samples studied

Sample I.D.*	Country	Basin	Well	Formation	Age	Depth
BB001C	China	—	—	—	—	—
BB002C	China	—	—	—	—	—
BB003C	China	—	—	—	—	—
BB004C	China	—	—	—	—	—
BB005C	China	—	—	—	—	—
BB006C	China	—	—	—	—	—
BB007C	China	—	—	—	—	—
CY001C	Argentina	Cuyo	YPF.Md.TBN e-3	Barrancas	L.–M Jur.	2975–3050 (m)
CY002C	Argentina	Cuyo	YPF.Md.PPC x-1	Potrerillos – Barrancas	M. Trias. – M Jur.	3048–3525 (m)
CY003C	Argentina	Cuyo	YPF.Md.PPC x-2	Potrerillos	M. Trias.	3711–3720 (m)
CY004C	Argentina	Cuyo	YPF.Md. B-332	Las Cabras – Barrancas	M. Trias. – M. Jur.	1968–2175 (m)
CY001B	Argentina	Cuyo	Outcrop	Cacheuta	Triassic	—
G1016B	U.S.A.	Piceance Creek	Shell 22X-1**	Green River	Eocene	1016–1018 (ft)
G1018B	U.S.A.	Piceance Creek	Shell 22X-1**	Green River	Eocene	1018–1020 (ft)
G1020B	U.S.A.	Piceance Creek	Shell 22X-1**	Green River	Eocene	1020–1022 (ft)
G1022B	U.S.A.	Piceance Creek	Shell 22X-1**	Green River	Eocene	1022–1024 (ft)
G1024B	U.S.A.	Piceance Creek	Shell 22X-1**	Green River	Eocene	1024–1026 (ft)
G1026B	U.S.A.	Piceance Creek	Shell 22X-1**	Green River	Eocene	1026–1028 (ft)
G1028B	U.S.A.	Piceance Creek	Shell 22X-1**	Green River	Eocene	1028–1030 (ft)
G1030B	U.S.A.	Piceance Creek	Shell 22X-1**	Green River	Eocene	1030–1032 (ft)
G1032B	U.S.A.	Piceance Creek	Shell 22X-1**	Green River	Eocene	1032–1034 (ft)
G1034B	U.S.A.	Piceance Creek	Shell 22X-1**	Green River	Eocene	1034–1036 (ft)
G2020B	U.S.A.	Piceance Creek	Shell 22X-1**	Green River	Eocene	2020–2022 (ft)
G2022B	U.S.A.	Piceance Creek	Shell 22X-1**	Green River	Eocene	2022–2024 (ft)
G2024B	U.S.A.	Piceance Creek	Shell 22X-1**	Green River	Eocene	2024–2026 (ft)
G2026B	U.S.A.	Piceance Creek	Shell 22X-1**	Green River	Eocene	2026–2028 (ft)
G2028B	U.S.A.	Piceance Creek	Shell 22X-1**	Green River	Eocene	2028–2030 (ft)
G2030B	U.S.A.	Piceance Creek	Shell 22X-1**	Green River	Eocene	2030–2032 (ft)
G2032B	U.S.A.	Piceance Creek	Shell 22X-1**	Green River	Eocene	2032–2034 (ft)
G2034B	U.S.A.	Piceance Creek	Shell 22X-1**	Green River	Eocene	2034–2036 (ft)
G2036B	U.S.A.	Piceance Creek	Shell 22X-1**	Green River	Eocene	2036–2038 (ft)
G2038B	U.S.A.	Piceance Creek	Shell 22X-1**	Green River	Eocene	2038–2040 (ft)
G2040B	U.S.A.	Piceance Creek	Shell 22X-1**	Green River	Eocene	2040–2042 (ft)
G2528B	U.S.A.	Piceance Creek	Shell 22X-1**	Green River	Eocene	2528–2530 (ft)
G2530B	U.S.A.	Piceance Creek	Shell 22X-1**	Green River	Eocene	2530–2532 (ft)
G2532B	U.S.A.	Piceance Creek	Shell 22X-1**	Green River	Eocene	2532–2534 (ft)
G2534B	U.S.A.	Piceance Creek	Shell 22X-1**	Green River	Eocene	2534–2536 (ft)
G2536B	U.S.A.	Piceance Creek	Shell 22X-1**	Green River	Eocene	2536–2538 (ft)
G2538B	U.S.A.	Piceance Creek	Shell 22X-1**	Green River	Eocene	2538–2540 (ft)
G2540B	U.S.A.	Piceance Creek	Shell 22X-1**	Green River	Eocene	2540–2542 (ft)
G2542B	U.S.A.	Piceance Creek	Shell 22X-1**	Green River	Eocene	2542–2544 (ft)
G2544B	U.S.A.	Piceance Creek	Shell 22X-1**	Green River	Eocene	2544–2546 (ft)
G2546B	U.S.A.	Piceance Creek	Shell 22X-1**	Green River	Eocene	2546–2548 (ft)
G2548B	U.S.A.	Piceance Creek	Shell 22X-1**	Green River	Eocene	2548–2550 (ft)
G2550B	U.S.A.	Piceance Creek	Shell 22X-1**	Green River	Eocene	2550–2552 (ft)
G2552B	U.S.A.	Piceance Creek	Shell 22X-1**	Green River	Eocene	2552–2554 (ft)
G2554B	U.S.A.	Piceance Creek	Shell 22X-1**	Green River	Eocene	2554–2556 (ft)

* Last character of sample identification designates: B = Bitumen; C = Crude Oil.** U.S.G.S. No. C177.

Table 2. Carbon isotopic compositons (‰ vs PDB) of saturate and aromatic fractions of crude oils and bitumens

Sample	$\delta^{13}C_{sat}$ (‰)	$\delta^{13}C_{aro}$ (‰)	$\Delta\delta_{aro\text{-}sat}$ (‰)
BB001C	− 32.70	− 30.95	1.75
BB002C	− 31.30	− 30.50	0.80
BB003C	− 32.60	− 30.50	2.10
BB004C	− 32.90	− 30.30	2.60
BB005C	− 32.10	− 30.90	1.20
BB006C	− 34.65	− 30.80	3.85
BB007C	− 32.10	− 30.40	1.70
CY001C	− 31.00	− 28.80	2.20
CY002C	− 30.30	− 28.30	2.00
CY003C	− 28.30	− 26.50	1.80
CY004C	− 32.30	− 29.40	1.90
CY001B	− 38.20	− 32.20	6.00
G1016B	− 33.50	− 30.30	3.20
G1026B	− 33.80	− 30.40	3.40
G1030B	− 34.70	− 30.30	4.40
G1032B	− 35.10	− 30.50	4.60
G2020B	− 33.60	− 31.40	2.20
G2024B	− 33.80	− 31.40	2.40
G2032B	− 33.90	− 31.40	2.50
G2534B	− 33.70	− 31.30	2.40
G2546B	− 33.80	− 31.40	2.40
G2554B	− 33.50	− 31.40	2.10

the saturate and aromatic fractions (expressed as $\Delta\delta_{aro\text{-}sat}$) range between 0.80 and 6.0‰ (Table 2). In each sample set, ^{13}C contents for the saturate fractions show greater variation than the aromatic fractions. This observation is particularly striking for the Chinese lacustrine oils and samples from the Cuyo Basin (Figs 1 and 2). Isotopic compositions of the saturate and aromatic fractions for samples from the Cuyo Basin show a strong covariance whereas $\delta^{13}C$ values for the remaining samples are relatively invariant (Figs 1 and 2).

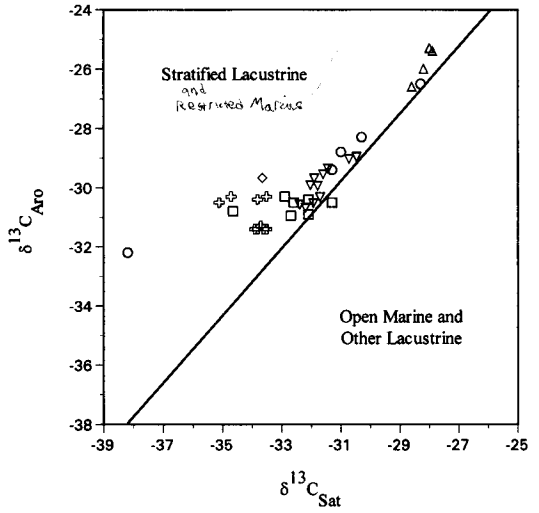

Fig. 1. Carbon isotopic composition of aromatic vs saturate fractions of lacustrine oils and bitumens. (□ = Chinese lacustrine oils; ○ = Cuyo Basin oils and bitumens; ✣ = Green River bitumens; ▽ = Uinta Basin oils (data from Sofer, 1984); ◇ = Messel oil shale (data from Hayes *et al.*, 1987); △ = Mae Sot oil shale (data from Curiale and Gibling (1994)). The line represents the best fit separation for waxy and non-waxy oils and is described by the equation $\delta^{13}C_{aro} = 1.14\delta^{13}C_{sat} + 5.46$ (after Sofer, 1984).

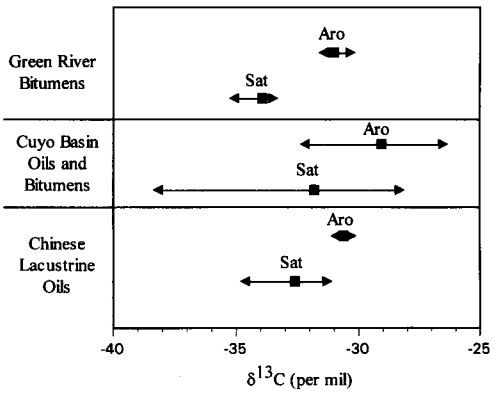

Fig. 2. Ranges of $\delta^{13}C$ values (‰ vs PDB) for saturate and aromatic fractions of lacustrine oils and bitumens. (Closed squares indicate the average $\delta^{13}C$ composition for each data set and arrows represent the range).

For all samples, depletions in ^{13}C for the saturated hydrocarbon fraction are observed to coincide with hopane abundance. The $\Delta\delta_{aro\text{-}sat}$ values for all samples correlate strongly with the quantitative hopane abundance in the saturate fraction (Fig. 3). This suggests that the isotopic depletion in the saturate fraction relative to the aromatic fraction is controlled largely by the isotopic compositions of the hopanes. To test this hypothesis, isotopic compositions of individual hopanes from the Green River bitumens (Table 3) were used to estimate the isotopic compositions of the hopane fractions. For samples with no analytical data, average values for each compound were used (Table 3). The isotopic compositions of the extended hopanes were averaged to provide an estimated $\delta^{13}C$ value for the pooled extended hopanes (C_{32} to C_{35} *R* and *S*; $\delta^{13}C = -47.4$‰). This simplification was justified by

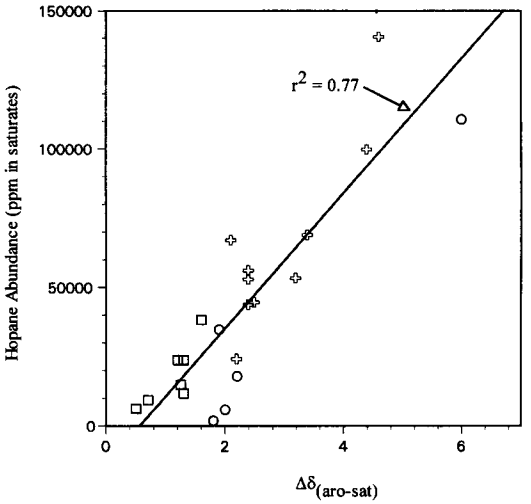

Fig. 3. Variation of hopane abundance (ppm in saturate fraction) with the $\Delta\delta_{aro\text{-}sat}$ value (‰ vs PDB) for lacustrine oils and bitumens. (□ = Chinese lacustrine oils; ○ = Cuyo Basin oils and bitumens; ✣ = Green River Formation bitumens).

the following considerations: the extended hopanes are quantitatively unimportant to the total hopane fraction ($X = 0.04 - 0.28$; Table 4), they appear to have homogeneous isotopic compositions (Table 3), and the isotope data for these compounds is limited due to their low abundances (Tables 3 and 4). The isotopic composition of the hopane fraction was estimated by the equation:

$$\delta^{13}C_{hopanes} = \sum \delta^{13}C_{compound}(X_{compound})$$

where X is the fractional abundance of each compound in the hopanes fraction (integrated from the m/z 191 trace). The compounds used in the calculation include the C_{29}–C_{35} hopanes and the C_{29} and C_{30} moretanes. The results of the calculation are summarized in Table 4 and are plotted against the $\Delta\delta_{aro\text{-}sat}$ values in Fig. 4. The model illustrates the point that the degree of depletion in the saturate fraction relative to the aromatic fraction is due largely to contributions from ^{13}C-depleted hopanoids.

Compound specific isotope analysis of extracts from the Green River Formation (Piceance Creek Formation), Gilsonite from the Uinta Basin, and the Messel shale revealed hopanes with extremely depleted $\delta^{13}C$ values (ca. -40 to -85‰; Freeman *et al.*, 1990; Collister *et al.*, 1992; Schoell *et al.*, 1994). Similar isotopic depletion for hopanes have been reported from sediments in a modern stratified lake (Spooner *et al.*, 1994). Such extreme ^{13}C-depletions for lipids can only be explained by biogenic input from methylotrophic bacteria utilizing methanogenic CH_4 ($\delta^{13}C = -50$ to -65‰ for most freshwater environments; Whiticar and Faber, 1986). Since methanotrophic bacteria thrive at the chemocline of stratified lakes (Hanson, 1980), the existence of extremely ^{13}C-depleted hopanes in geologic samples is evidence for paleostratification. The ^{13}C-depleted saturate fractions of lacustrine oils and source rock extracts are thus suggested to result largely from methanotrophic input to the sediments. The relatively ^{13}C-enriched saturate fractions from open marine oils are related to the abundant sulfate in marine environments. Sulfate reducers can outcompete methanogens for metabolic intermediates (Lovely and Klug, 1983) and, in marine environments, tend to attenuate the methane cycle.

It is worth noting that Summons *et al.* (1994) found significant amounts of other lipids (including methyl sterols and fatty acids) as components of methylotrophic bacteria. They observed that both hopanols and sterols were depleted in ^{13}C relative to the biomass by up to 10‰, whereas the fatty acids displayed lesser depletions. Thus, input of lipids other than hopanoids from methanotrophic bacteria will potentially influence the position of a sample on the Sofer-plot. Initially, these ^{13}C-depleted compounds would introduce light carbon into the NSO fraction, and thus do not influence the ^{13}C contents of the saturate and aromatic fractions. However, subsequent defunctionalization and saturation of these compounds during diagenesis and catagenesis, ultimately results in their contribution to the saturated hydrocarbon fraction of bitumens and crude oils. Therefore, although abundant ^{13}C-depleted hopanes are responsible primarily for high $\Delta\delta_{aro\text{-}sat}$ values in stratified lacustrine settings, contributions of isotopically light carbon from other methanotrophic bacterial lipids may reinforce the trend defined by the hopane fraction.

Unlike samples from open marine environments, $\Delta\delta_{aro\text{-}sat}$ values for oils and rocks deposited in restricted marine environments can be highly variable. Indeed, data reported for oils and source rocks from the Monterey Formation (Curiale *et al.*, 1985) plot in both sectors on the "Sofer-plot". Contributions of isotopicially depleted lipids from photosynthetic bacteria are likely to affect the ^{13}C contents of saturate fractions in samples from restricted marine environments. For example, in a Monterey crude oil, Schoell *et al.* (1992) report the occurrence of 28,30-bisnorhopane isomers that are depleted in ^{13}C by approximately 8‰ relative to lipids from photoautotrophic algae. Additionally, isotopically depleted diploptene ($\delta^{13}C = -41.2$‰) has been reported from a Black Sea sediment (Freeman *et al.*, 1994). This hopanoid is thought to derive from chemoautotrophic bacteria that live deep in the water column and consume ^{13}C depleted inorganic carbon (Freeman *et al.*, 1994). Thus, large contributions of lipids from these organisms could account for elevated $\Delta\delta_{aro\text{-}sat}$ values sometimes observed in samples from restricted marine environments. It should be noted that ^{13}C depletions observed in chemoautotrophic bacterial lipids are much less than those of methylotrophic lipids. Accordingly, contributions from chemoautotrophic organisms in restricted marine environments would have to be larger than contributions of methylotrophic lipids in stratified lacustrine settings, to account for saturate fractions that plot in the "stratified lacustrine" sector on the "Sofer-plot". In stratified lacustrine settings, the observed ^{13}C-depletion in the saturate fraction is driven by abundant hopanes with extreme ^{13}C depletions.

Since it is established that the oils and source rocks in Fig. 1 were deposited in a stratified lacustrine environment, the issue of salinity warrants additional comment. The samples plotted in Fig. 1 represent a broad range of salinities. Based on mineral assemblages, estimates of salinities for the Green River lakes are as high as ten times that of sea water (Bradley and Eugster, 1969). In contrast the depositional systems for the Messel oil shale, the Mae Sot oil shale and the Cacheuta Formation (Cuyo Basin) are thought to have contained freshwater (Matthess, 1968; Strelkov and Alvarez, 1984; Curiale and Gibling, 1994). Thus the isotopic depletion of the saturate fractions are the result of stratification rather

Table 3. Carbon isotopic compositions (‰ vs PDB) of individual hopanoids in Green River Formation bitumens

Sample	C_{29} Hopane	C_{29} Moretane	C_{30} Hopane	C_{30} Moretane	C_{31} Hop 20*S*	C_{31} Hop 20*R*	C_{32} Hop 20*S*	C_{32} Hop 20*R*	C_{33} Hop 20S	C_{33} Hop 20*R*
G1016B	− 54.8	− 61.1 ± 1.5	− 59.8 ± 0.2	− 59.4 ± 1.2	—	—	—	—	—	—
G1018B	− 54.4 ± 0.80	− 63.4 ± 0.18	− 59.0	− 58.2 ± 0.1	—	—	—	—	—	—
G1020B	− 52.8	− 60.6	− 52.9 ± 0.1	− 51.2 ± 0.1	—	—	—	—	—	—
G1022B	− 44.4	− 48.8	− 44.5	− 41.6	—	—	—	—	—	—
G1024B	− 43.8	− 52.8 ± 0.20	− 47.3 ± 0.1	− 44.3 ± 0.9	—	—	—	—	—	—
G1026B	− 49.8	− 63.2 ± 0.8	− 55.3 ± 0.8	− 55.2 ± 0.2	—	—	—	—	—	—
G1030B	—	− 68.0 ± 0.4	− 58.1 ± 0.2	—	—	—	—	—	—	—
G1032B	− 54.5 ± 0.3	− 67.7 ± 1.0	− 59.6 ± 1.1	—	—	—	—	—	—	—
G1034B	− 56.5 ± 0.6	− 72.8 ± 0.7	− 61.6 ± 0.1	—	—	—	—	—	—	—
G2020B	− 51.3 ± 1.3	− 53.4 ± 1.2	− 55.9 ± 1.2	—	—	—	—	—	—	—
G2022B	− 50.3 ± 0.1	− 59.5 ± 1.4	− 55.2 ± 0.4	—	− 49.3	− 54.2 ± 0.2	—	—	—	—
G2024B	− 49.6 ± 0.4	—	− 65.0 ± 0.2	—	− 49.1	− 52.0 ± 0.7	—	—	—	—
G2026B	− 48.0 ± 0.4	− 53.8 ± 3.0	− 54.9 ± 0.1	—	− 53.2	− 55.1 ± 2.3	—	—	—	—
G2032B	− 55.4 ± 0.52	—	− 60.1 ± 0.8	—	—	− 54.1 ± 1.3	—	—	—	—
G2036B	− 51.1 ± 1.1	− 49.6	− 54.9 ± 1.1	—	− 49.1	− 49.9 ± 0.4	—	—	—	—
G2038B	− 50.3 ± 0.2	− 51.6 ± 0.2	− 53.8 ± 0.5	—	− 54.6 ± 0.6	− 58.9 ± 0.2	− 43.9 ± 0.4	− 47.7 ± 1.3	—	—
G2040B	− 51.2 ± 1.3	—	− 56.0 ± 0.4	—	—	—	—	—	—	—
G2528B	− 50.3 ± 0.2	− 44.6 ± 2.0	− 52.3 ± 0.3	—	− 52.3 ± 1.0	− 52.0 ± 0.7	− 51.0 ± 0.5	− 46.8 ± 0.2	—	—
G2530B	—	—	− 49.9 ± 0.5	− 64.2 ± 0.0	− 49.1 ± 0.9	− 47.5 ± 2.1	− 45.4 ± 0.2	− 44.6 ± 1.9	—	—
G2532B	− 45.3	− 44.9	− 51.6	− 59.0	− 46.5 ± 0.5	− 44.7 ± 0.9	—	—	—	—
G2534B	− 48.5 ± 0.7	− 42.7 ± 1.0	− 49.7 ± 0.8	—	− 50.2 ± 1.5	− 49.5 ± 1.5	− 47.1 ± 0.4	− 43.7 ± 0.5	− 48.3 ± 0.4	− 44.6 ± 0.51
G2536B	− 47.7 ± 0.60	− 41.6	− 51.7 ± 0.9	− 64.9 ± 0.3	− 53.3 ± 0.9	− 54.2 ± 0.1	− 49.5 ± 0.4	− 49.6 ± 1.7	− 49.6 ± 0.2	− 48.9 ± 1.5
G2538B	− 49.0 ± 0.40	—	− 51.7 ± 0.5	− 49.2	− 49.0 ± 0.1	− 48.9 ± 1.0	− 43.4 ± 0.3	− 46.6 ± 0.5	− 44.6 ± 0.3	− 44.4 ± 0.2
G2540B	− 46.2 ± 0.44	—	− 52.7 ± 0.2	− 60.6 ± 0.8	− 48.4 + 0.1	− 47.6 ± 0.2	− 44.5 ± 0.1	− 48.7 ± 0.1	− 46.7 ± 1.6	− 47.0 ± 1.6
G2542B	− 45.9 ± 0.28	− 43.6 ± 2.5	− 52.8 ± 0.4	− 59.3 ± 0.5	− 47.4 ± 0.3	− 47.9 ± 0.3	− 42.1 ± 0.3	− 45.8 ± 1.7	− 45.1 ± 0.1	− 45.2 ± 1.7
G2544B	− 44.0 ± 0.78	− 43.4 ± 0.3	− 49.5 ± 0.5	− 58.6 ± 1.1	− 45.5 ± 0.2	− 45.7 ± 0.1	− 42.6 ± 1.2	− 46.6 ± 0.3	− 45.2 ± 0.	− 44.9 ± 0.5
G2546B	− 43.5 ± 0.21	− 45.5 ± 0.1	− 52.2 ± 0.2	− 62.1 ± 0.3	− 47.6 ± 0.2	− 48.9 ± 0.4	− 44.6 ± 1.4	− 48.4 ± 0.5	− 47.3 ± 0.8	− 46.2 ± 0.5
G2548B	− 44.4 ± 3.15	− 43.2 ± 0.6	− 49.3 ± 0.1	− 58.3 ± 1.0	− 45.6 ± 0.1	− 43.6 ± 0.1	− 41.1 ± 0.7	− 43.5 ± 0.6	− 43.9 ± 0.4	− 42.6 ± 1.5
G2550B	− 50.1 ± 0.58	− 44.0 ± 0.8	− 52.1 ± 0.1	− 59.9 ± 3.3	− 46.3 ± 1.9	− 46.3 ± 1.7	− 48.3 ± 2.4	− 46.5 ± 0.7	− 50.3 ± 0.2	− 47.6 ± 1.6
G2552B	− 50.1 ± 0.58	—	− 52.7 ± 0.2	—	—	—	—	—	—	—
G2554B	—	—	—	—	− 50.0 ± 0.3	− 51.1 ± 0.6	− 45.5 ± 0.2	− 47.7 ± 0.2	− 48.7 ± 0.2	− 46.2 ± 2.2
Ave.	− 49.5	− 52.8	− 54.2	− 57.3	− 48.8	− 50.3	− 46.0	− 46.6	− 47.0	− 45.8

Table 4. Estimated carbon isotopic compositions of 'hopane fractions', fractional abundances of hopanes in the hopane fraction and maturity parameters for crude oils and bitumens

Sample	$\delta^{13}C$ Hops.*	Fractional abundance**						Hopanes (ppm in sats)	C_{29} Steranes $20S/(20S+20R)$	C_{31} Hopanes $22S(22S+22R)$
		C_{29} H	C_{29} M	C_{30} H	C_{30} M	C_{31} H(R&S)	$\Sigma C_{32\,35}$ H(R&S)			
BB001C	—	0.144	0.020	0.483	0.064	0.130	0.159	14846	0.38	0.60
BB002C	—	0.146	0.023	0.440	0.062	0.143	0.186	6202	0.39	0.59
BB003C	—	0.153	0.028	0.492	0.073	0.112	0.142	23726	0.26	0.55
BB004C	—	0.151	0.021	0.473	0.064	0.134	0.157	23742	0.35	0.56
BB005C	—	0.150	0.028	0.478	0.065	0.120	0.159	9238	0.30	0.56
BB006C	—	0.148	0.020	0.471	0.064	0.132	0.165	38296	0.34	0.55
BB007C	—	0.112	0.022	0.463	0.071	0.138	0.194	11736	0.35	0.56
CY001C	—	0.247	0.017	0.461	0.029	0.129	0.117	17905	0.45	0.57
CY002C	—	0.031	0.031	0.577	0.048	0.157	0.156	5801	0.51	0.57
CY003C	—	0.272	0.028	0.404	0.058	0.134	0.134	1827	0.51	0.57
CY004C	—	0.293	0.026	0.417	0.039	0.121	0.104	34703	0.35	0.58
CY001B	—	0.200	0.091	0.521	0.054	0.101	0.033	110698	0.09	0.39
G1016B	− 58.3	0.087	0.074	0.561	0.189	0.051	0.038	53353	0.27	0.34
G1026B	− 57.7	0.075	0.061	0.614	0.185	0.029	0.036	68913	0.25	0.28
G1030B	− 57.2	0.073	0.056	0.637	0.177	0.032	0.025	99780	0.23	0.33
G1032B	− 58.5	0.069	0.056	0.646	0.171	0.029	0.029	140435	0.23	0.29
G2020B	− 52.5	0.176	0.062	0.367	0.110	0.107	0.178	24144	0.33	0.45
G2024B	− 55.4	0.167	0.062	0.363	0.109	0.108	0.191	43705	0.33	0.46
G2032B	− 54.7	0.175	0.063	0.364	0.112	0.107	0.179	44575	0.34	0.46
G2534B	− 48.6	0.184	0.037	0.334	0.068	0.116	0.261	52862	0.38	0.57
G2546B	− 49.0	0.176	0.037	0.333	0.069	0.118	0.267	56081	0.36	0.57
G2554B	− 50.6	0.169	0.034	0.330	0.067	0.121	0.279	66988	0.34	0.57

* Estimated from the data in Table 3 using the equation: $\delta^{13}C_{hopanes} = \Sigma\delta^{13}C_{compound}(X_{compound})$.** Fractional abundances within 'hopane fraction': integrated from m/z 191; H = hopane, M = Moretane.

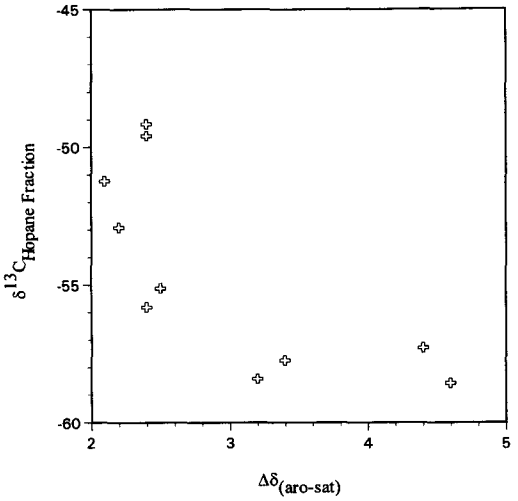

Fig. 4. Variation of the calculated $\delta^{13}C$ values for the "hopane fraction" (see text) with the $\Delta\delta_{aro\text{-}sat}$ value (‰ vs PDB) for Green River bitumens.

than a function of salinity per se. This is in accordance with recent publications that indicate that other features typical of lacustrine organic material (e.g. elevated gammacerane indices) result from density stratification rather than salinity (Schoell *et al.*, 1994; Sinninghe Damsté *et al.*, 1995).

A plot of the $\Delta\delta_{aro\text{-}sat}$ vs the C_{29} sterane isomerization (Fig. 5) shows the effect of maturity on the isotopic compositions of the saturate fraction. Indeed, $\Delta\delta_{aro\text{-}sat}$ decreases with increasing thermal stress. In immature samples, the extractable hydrocarbons are likely to derive from free lipids, whereas lipids in mature sedimentary rocks are dominated generally by catagenically released hydrocarbons from the kerogen matrix (Collister *et al.*, 1992; Bjorøy *et al.*, 1992). *n*-Alkanes in Green River pyrolyzates contain ^{13}C contents between -26.9 and -33.3‰ (Eglinton *et al.*, 1991; Bjorøy *et al.*, 1992; Collister *et al.*, 1992). Further, it has been demonstrated that hopanes released during pyrolysis of Green River Formation kerogens are enriched in ^{13}C relative to the free hopanes found in extracts from the same samples (Eglinton *et al.*, 1991; Bjorøy *et al.*, 1992). Thus, it follows that the hopane fraction in extracts of the Green River Formation should become increasingly enriched in ^{13}C with increasing maturation (Table 4). Further, increased contributions of other lipids to the saturate fraction (e.g., *n*-alkanes) will dilute the isotopic signal from the hopanes resulting in ^{13}C-enriched saturate fractions. If these relationships hold for other petroleum systems, it will follow that the separation of lacustrine samples on the modified "Sofer-plot" will be affected by maturity and that the plot will be less effective in categorizing samples that have experienced high levels of thermal stress. That these relationships are demonstrated to be valid on four continents contributes to the hypothesis that this is a global phenomenon.

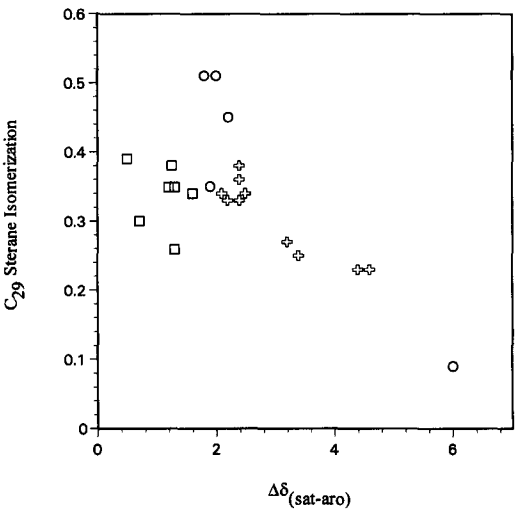

Fig. 5. Variation of the $\alpha\alpha\alpha$ ethylcholestane isomerization ($20S/(20S + 20R)$) with the $\Delta\delta_{aro\text{-}sat}$ value (‰ vs PDB) for lacustrine oils and bitumens. (□ = Chinese lacustrine oils; ○ = Cuyo Basin oils and bitumens; = Green River Formation bitumens).

CONCLUSIONS

The modified "Sofer-plot" is an effective tool to differentiate stratified lacustrine depositional settings from open marine and non-stratified lacustrine settings. The displacement from the best fit line on the plot results from methanotrophic input of isotopically depleted lipids to the saturate fraction. In open marine systems, abundant sulfate and sulfate reduction serve to attenuate the methane cycle and methanotrophic input is minimized. The displacement on the "Sofer-plot" can be affected by thermal stress such that immature samples show the greatest shift from the best-fit line.

Associate Editor—**K. Freeman**

Acknowledgements—The authors wish to thank W. H. Kanes of the Earth Sciences and Resources Institute at the University of Utah for providing the opportunity to pursue this fundamental research. Individuals that provided the samples are also greatly acknowledged: J. Dyni of the U.S.G.S. (Denver, Colorado), D. Schumacher of Pennzoil (Houston, Texas) / E.S.R.I. (Salt Lake City, Utah), and M. A. Turic of YPF S.A. (Buenos Aires, Argentina). J. M. Hayes and K. H. Freeman are sincerely thanked for their constructive reviews of this manuscript.

REFERENCES

Bjorø M., Hall P. B., Hustad E. and Williams J. A. (1992) Variation in stable carbon isotope ratios of individual hydrocarbons as a function of artificial maturity. *Org. Geochem.* **19,** 89–105.

Bradley W.H. and Eugster H.P. (1969) Geochemistry and paleolimnology of the trona deposits and associated authigenic minerals of the Green River Formation, Wyoming. *U.S. Geol. Survey Prof. Paper* **496-B,** 71 pp.

Chung H. M., Brand S. W. and Grizzle L. (1981) Carbon isotope geochemistry of Paleozoic oils from Big Horn Basin. *Geochim. Cosmochim. Acta* **45,** 1803–1815.

Collister J. W., Summons R. E., Lichtfouse E. L. and Hayes J. M. (1992) An isotopic bio-geochemical study of the Green River oil shale. *Org. Geochem.* **19,** 265–276.

Curiale J. A. and Gibling M. R. (1994) Productivity control on oil shale formation—Mae Sot Basin, Thailand. *Org Geochem.* **21,** 67–89.

Curiale J. A., Douglas C. and Davis D. V. (1985) Biological marker distribution and significance in oils and rocks of the Monterey Formation, California. *Geochim. Cosmochim. Acta* **49,** 271–288.

Eglinton T. I., Fry B. D., Freeman K. H. and Hayes J. M. (1991) Carbon-isotopic compositions of products from flash pyrolysis of kerogens. In *Organic Geochemistry. Advances and Applications in Energy and the Natural Environment* (Edited by Manning D.), pp. 411–416. Manchester University Press, Manchester–New York.

Freeman K. H., Hayes J. M., Trendel J.-M. and Albrecht P. (1990) Evidence from carbon isotope measurements for diverse origins of sedimentary hydrocarbons. *Nature* **343,** 254–256.

Freeman K. H., Wakeham S. G. and Hayes J. M. (1994) Predictive isotopic biogeochemistry: hydrocarbons from anoxic marine basins. *Org. Geochem.* **21,** 629–644.

Hanson (1980) Ecology and diversity of methylotrophic organisms. *Adv. Appl. Microbiol.* **26,** 3–37.

Hayes J. M., Takigiku R., Ocampo R., Callot H. J. and Albrecht P. (1987) Isotopic compositions and probable origins of organic molecules in the Eocene Messel shale. *Nature* **329,** 48–51.

Lovely D. R. and Klug M. J. (1983) Sulfate reducers can outcompete methanogens at freshwater sulfate concentrations. *Appl. Environ. Microbiol.* **45,** 187–192.

Matthess G. (1968) Les couches eocenes dans la region du Fosse rhenan septentrional. *Memoires du Bureau Rech. Geol. Min.* **58,** 327–338.

Matthews D. E. and Hayes J. M. (1978) Isotope-ratio-monitoring gas chromatography–mass spectrometry. *Anal. Chem.* **50,** 1465–1473.

Merritt D. A., Brand W. A. and Hayes J. M. (1994) Isotope-ratio-monitoring gas chromatography–mass spectrometry: methods for isotopic calibration. *Org. Geochem.* **21,** 573–583.

Schoell M., McCaffrey M. A., Fago F. J. and Moldowan J. M. (1992) Carbon isotopic compositions of 28,30-bisnorhopanes and other biological markers in Monterey crude oil. *Geochim. Cosmochim. Acta* **56,** 1391–1399.

Schoell M., Hwang R. J., Carlson R. M. K. and Welton J. E. (1994) Carbon isotopic compositions of individual biomarkers in gilsonites (Utah). *Org. Geochem.* **21,** 673–683.

Sinninghe Damsté J. S., Kenig F., Koopmans M. P., Koster J., Schouten S., Hayes J. M. and de Leeuw J. W. (1995) Evidence for gammacerane as an indicator of water column stratification. *Geochim. Cosmochim. Acta* **59,** 1895–1900.

Sofer Z. (1984) Stable carbon isotope compositions of crude oils: application to source depositional environments and petroleum alteration. *Am. Assoc. Petrol. Geol. Bull.* **68,** 31–49.

Spooner N., Rieley G., Collister J. W., Lander M., Cranwell P. A. and Maxwell J. R. (1994) Stable carbon isotopic correlation of individual biolipids in aquatic organisms and a lake bottom sediment. *Org. Geochem.* **21,** 823–827.

Stahl W. J. (1978) Source rock-crude oil correlation by isotopic type-curves. *Geochim. Cosmochim. Acta* **42,** 1573–1577.

Strelkov E. E. and Alvarez L. A. (1984) Análisis estratigráfico y evolutivo de la Cuenca Triasica Mendocina-Sanjuanina. IX Congr. Geol. Argentino, S.C. Bariloche, Actas VII, p. 115–130.

Summons R. E., Jahnke L. L. and Roksandik Z. (1994) Carbon isotopic fractionation in lipids from methanotrophic bacteria: relevance for interpretation of the geochemical record of biomarkers. *Geochim. Cosmochim. Acta* **58,** 2853–2863.

Whiticar M. J. and Faber E. (1986) Methane oxidation in sediments and water column environments—isotope evidence. *Org. Geochem.* **10,** 759–768.